X-ray absorption spectroscopy to watch catalysis by metalloenzymes: status and perspectives discussed for the water-splitting manganese complex of photosynthesis

Holger Dau* and Michael Haumann

Freie Universität Berlin, FB Physik, Arnimallee 14, D-14195 Berlin, Germany. E-mail: holger.dau@physik.fu-berlin.de

Understanding structure–function relations is one of the main interests in the molecular biosciences. X-ray absorption spectroscopy of biological samples (BioXAS) has gained the status of a useful tool for characterization of the structure of protein-bound metal centers with respect to the electronic structure (oxidation states, orbital occupancies) and atomic structure (arrangement of ligand atoms). Owing to progress in the performance characteristics of synchrotron radiation sources and of experimental stations dedicated to the study of (ultra-dilute) biological samples, it is now possible to carry out new types of BioXAS experiments, which have been impracticable in the past. Of particular interest are approaches to follow biological catalysis at metal sites by characterization of functionally relevant structural changes. In this article, the first steps towards the use of BioXAS to 'watch' biological catalysis are reviewed for the water-splitting reactions occurring at the manganese complex of photosynthesis. The following aspects are considered: the role of BioXAS in life sciences; methodological aspects of BioXAS; catalysis at the Mn complex of photosynthesis; combination of EXAFS and crystallographic information; the freeze-quench technique to capture semi-stable states; time-resolved BioXAS using a freeze-quench approach; room-temperature experiments and 'real-time' BioXAS; tasks and perspectives.

Keywords: bioinorganic chemistry; BioXAS; EXAFS; metalloenzymes; X-ray absorption spectroscopy.

1. Introduction

1.1. The role of BioXAS in life sciences

Understanding structure–function relations of biological macromolecules, their cofactors and substrate molecules is one of the main interests in the molecular biosciences. An estimated 30–50% of all enzymes carry protein-bound metal centers located mostly at the center of the catalytic site; essentially, all proteins involved in the various bioenergetic pathways (*e.g.* photosynthesis and respiration) are metalloenzymes (Lippard & Berg, 1994; Cowan, 1996; Hill *et al.*, 1999). X-ray absorption spectroscopy of biological samples (BioXAS) has gained the status of a useful tool for characterization of the structure of protein-bound metal centers (Yachandra, 1995; Scott, 2000). The method is particularly suitable for investigations of the highly interesting changes in electronic structure (oxidation states) and atomic structure (arrangement of ligand atoms) of the metal center that typically accompany transitions between various 'states' of the metal site. Owing to the tremendous progress in the performance characteristics of synchrotron radiation sources and of experimental stations dedicated to the study of (ultra-dilute) biological samples, it is now possible to carry out new types of BioXAS experiments, which have been impracticable in the past. Of particular interest are approaches to follow biological catalysis at metal sites by characterization of functionally relevant structural changes. In this article, the first steps towards the use of BioXAS to 'watch' biological catalysis are discussed for the water-splitting reactions occurring at the manganese complex of photosynthesis (Penner-Hahn, 1999; Robblee *et al.*, 2001; Dau *et al.*, 2001).

Today, protein crystallography is undoubtedly the best established and most prominent method for structure determination at near-atomic resolution. Nonetheless, experimental approaches are needed to complement protein crystallography and to overcome its limitations (as discussed in the following).

Recently, crystallographic structure determination has been successful for two large membrane-intrinsic cofactor-protein complexes that are particularly important for life on Earth: (i) photosystem II (PSII) (Zouni *et al.*, 2001), which facilitates the use of water as a substrate for the creation of organic matter by photosynthesis and produces, as a by-product, atmospheric dioxygen; and (ii) the cytochrome oxidase (COX) (Iwata *et al.*, 1995; Tsukihara *et al.*, 1996), which in living organisms facilitates the use of dioxygen to gain energy for the 'burning' of organic matter at physiological temperatures. Both protein complexes use several protein-bound metal centers to achieve their astonishing performance characteristics; in both cases the catalytic processes involving these metal centers are extremely complex.

A closer view of these two impressive success stories of protein crystallography also teaches some sobering lessons. (i) It took decades to achieve the crystallographic structure determination for these non-soluble membrane proteins. (ii) At least in the case of PSII, the achieved resolution is insufficient to provide unambiguous atomic resolution models of the active metal sites. The situation might improve in the future, but it is unlikely that the coordinates and chemical identities of all atoms (including protons) can be determined solely by protein crystallography at a resolution sufficient for, for example, quantum-chemical calculations on the catalytic mechanism. (iii) The crystallographic results provide only limited insights into the 'electronic structure' (oxidation states, orbital occupancies *etc.*), which is clearly important for enzymatic catalysis. (iv) The determination of the structure of the enzyme for only one 'resting state' or a limited number of states is not sufficient to understand the mechanism of catalysis. It has become clear that we need to 'watch' as closely as possible, and under a variety of experimental conditions (pH, temperature, inhibitors *etc.*), the advancement of the enzyme through its catalytic cycle. Without information on the relevant changes in nuclear coordinates and electronic structure, the catalytic mechanism necessarily remains only insufficiently understood.

By using advanced spectroscopic techniques (Sauer, 1995), it may become possible to partially overcome the above-mentioned limitations of the conventional crystallographic approach. BioXAS is likely to play a particularly prominent role in the efforts to understand the catalytic mechanisms of the numerous metalloenzymes found in living organisms. In this review, we focus on the attempt to 'watch' biological catalysis at metal sites using BioXAS.

Owing to the stochastic character of the movement along the reaction coordinates, it is obviously impossible to 'watch' literally the catalytic process. What we can achieve is the characterization of the atomic and electronic structure of various 'states' of the enzyme and the determination of the probability (rate constants) for transitions between states. Each 'state' represents the ensemble average of all the enzymes in sufficiently similar atomic and electronic conformations (or configurations). The meaning of 'sufficiently similar'

depends on the experimental method used and the question we intend to answer.

States of interest for elucidation of the catalytic mechanism are (i) semi-stable intermediates of the catalytic cycle investigated for various sets of environmental variables (pH, ion concentrations, temperatures *etc.*); (ii) catalytically 'non-functional' states (intermediate states in the assembly and disassembly process, inactive states involved in regulation of the catalytic activity; catalytic site modified by mutagenic exchange of amino-acid residues *etc.*); (iii) states populated in the course of 'titration curves' (pH, redox potential, substrate concentration); (iv) transition states stabilized by appropriate inhibitors (*e.g.* substrate analogs with inhibitor effects). The structural changes upon transition between states can be investigated by direct comparison of spectra of 'pure' states (§§2.2, 2.4) or by kinetic studies (*e.g.* time-resolved BioXAS), which also provide information on the transition rates (§2.3).

1.2. BioXAS – methodical aspects

BioXAS studies mostly involve measurements at the *K*-edge of protein-bound transition metals (Yachandra, 1995; Scott, 2000). [There are notable exceptions: for example, XAS at the bromine or selenium *K*-edge to investigate substrate binding (Dau *et al.*, 1999; Peariso *et al.*, 2001).] By the choice of a specific X-ray edge, the method facilitates specific investigation of the X-ray-absorbing element and its ligand environment (first few coordination spheres). *L*-edge XAS studies in the soft X-ray region can provide insights into the electronic structure of metal sites that are complementary to the information from *K*-edge XAS and EPR (Wang *et al.*, 1997, 2000; Cramer *et al.*, 1998; DeBeer George *et al.*, 2001). Typically, the ratio between the numbers of investigated metal atoms and host atoms (meaning the atoms of the proteins and the solvent) falls in the range 10000–100000. To cope with the background absorption of the matrix atoms, mostly the excitation spectra of the X-ray fluorescence are recorded using energy-resolving solid-state detectors. These fluorescence excitation spectra are free of the huge absorption background stemming from the matrix atoms; otherwise the excitation spectra are essentially identical to the *K*-edge absorption spectra. The desirable signal-to-noise ratio (with regard to the total X-ray absorption coefficient) is of the order of 10^2 for XANES and 10^3–10^4 for EXAFS spectra (at the end of the EXAFS range). Today, using reasonably intense X-rays, a fluorescence detection mode and averaging of several energy scans (3–100), such high-quality XAS data can be obtained for protein-bound metal centers. At a typical bending-magnet beamline it may take 12–24 h to obtain a single high-quality EXAFS spectrum. Owing to progress at the synchrotron radiation sources, the time needed to obtain one high-quality spectrum is continuously decreasing (by orders of magnitude, see also §2.4), thereby significantly increasing the potential of BioXAS for fruitful investigations on biological catalysis.

In principle, BioXAS can be used to investigate protein-bound metal centers of any kind in all states of the enzyme; the method is restricted to neither specific elements nor specific oxidation states. Metalloenzymes in solution and metal centers in proteins that are embedded in their native membrane environment can be studied. Today, high-quality BioXAS measurements are also feasible at room temperature using 'quasi-physiological' experimental conditions (Meinke *et al.*, 2000; see §2.4).

The pre-edge and edge regions (XANES) of the X-ray absorption spectrum carry information on the electronic structure and atomic structure of the metal site. Typically, the information content of these regions of the spectrum is exploited in the form of a comparative analysis (mostly by comparison with synthetic models), but not by simulations based on established theoretical grounds (for manganese see *e.g.* Penner-Hahn, 1999; Kirby, Goodin *et al.*, 1981; Kirby, Robertson *et al.*, 1981; Sauer *et al.*, 1992; Bossek *et al.*, 1996; Dittmer *et al.*, 1998). However, owing to improved theoretical approaches, a more rigorous treatment of the XANES region may be within reach (see *e.g.* Ankudinov *et al.*, 2001).

In contrast to the edge range, the fine structure observed in X-ray absorption spectra for energies above the edge (EXAFS) is well understood. Using well established theoretical approaches (Gurman *et al.*, 1984; Rehr *et al.*, 1991; Filliponi *et al.*, 1991), analysis of EXAFS spectra can also facilitate (partial) solution of the inverse problem (meaning the determination of structure based on spectra) in a relatively straightforward way. Typically, the small oscillatory EXAFS structure is extracted by subtraction of a smooth background from the previously normalized spectra before transformation of the energy to a wavenumber scale (Teo, 1986). The subsequently Fourier-transformed wavenumber spectra already provide information on the distance between absorbing atom and backscattering atoms of the first coordination spheres. Fourier transforms allow an often instructive visualization and rough qualitative evaluation of the structural information carried by the EXAFS spectrum (therefore, in the following, exclusively Fourier-transformed EXAFS spectra are shown). Simulation of spectra (curve fitting) is required to obtain detailed structural information.

The EXAFS is related to the backscattering of electrons set free at the X-ray-absorbing atom by nearby ligand atoms (Teo, 1986). Consequently, the X-ray-absorbing atom is often denoted as the 'absorber', whereas the ligands of the first few coordination spheres (or shells) of the absorbing atom are denoted as 'backscatterers' or 'backscattering atoms'. Frequently, average distances, R_i, between the absorbing atom and the backscattering atoms of the first, second and occasionally also higher coordination spheres can be determined with a precision of 0.01–0.03 Å. The accuracy in the determined number of backscattering atoms (coordination number), N_i, is significantly lower (about 25%), because this parameter may be highly correlated with the corresponding Debye–Waller parameter (σ_i), which describes the distance spread in the coordination sphere. In the case of highly heterogeneous backscattering shells (meaning various types of backscattering atoms or a significantly non-Gaussian distance spread within one coordination sphere), it is often impossible to obtain reliable estimates of the coordination numbers without using constraints or additional assumptions (σ_i fixed to reasonable values, restriction to chemically reasonable approaches, sequence information *etc.*). The use of 'chemically reasonable' assumptions is not necessarily unproblematic; misleading results were obtained in early XAS investigations on cytochrome oxidase and nitrogenase.

In protein crystallography, the model building typically involves knowledge of the structure of the individual amino-acid residues. In addition, in the case of BioXAS, the formulation of structural models is necessarily guided by insights into the chemical feasibility of structural motifs. Fortunately, knowledge about conceivable structural motifs and their potential mechanistic role is growing rapidly because of the activities of numerous synthetic chemists. For example, in synthetic compounds, Mn—Mn distances of 2.65–2.75 Å are almost exclusively found for unprotonated di-μ-oxo-bridged binuclear Mn units (Wieghardt, 1989; Pecoraro, 1992; Armstrong, 1992); in these units the Mn—μO distance is around 1.8 Å. Seemingly, Mn—Mn distances of around 2.7 Å are characteristic for pairs of Mn ions connected by unprotonated di-μ-oxo bridges. Spectra of the PSII manganese (see below) complex in its S_1 state indicate the presence of Mn—Mn distances of 2.71 (0.03) Å in this tetramanganese

complex; the amplitude of the associated EXAFS suggests the presence of more than one 2.7 Å Mn—Mn vector per complex (Kirby, Goodin *et al.*, 1981; Kirby, Robertson *et al.*, 1981; Yachandra *et al.*, 1986; Penner-Hahn *et al.*, 1990; MacLachlan *et al.*, 1992; Schiller *et al.*, 1998). Therefore, it has been concluded that the Mn complex contains two pairs of di-μ-oxo-bridged binuclear Mn units (Sauer *et al.*, 1992; Yachandra *et al.*, 1993), a conclusion that is in agreement with the relatively short Mn–ligand distances found by simulation of the EXAFS oscillations associated with the first-coordination sphere. These di-μ-oxo bridges are assumed to be fully unprotonated because in $Mn_2(\mu-O)(\mu-OH)$ complexes the Mn—Mn distance is found to be around 2.8 Å (Larson *et al.*, 1992). This example demonstrates how the combination of EXAFS data and insights obtained by model chemistry allows the formulation of detailed structural models; even a distinction between various protonation states of ligands may become possible.

In the following we will review our recent experiments on light-driven water oxidation by the photosystem II manganese complex. Using this 'test system', the current status of the use of BioXAS for investigations on transitions between various states of the metal center is discussed.

1.3. Catalysis at the Mn complex of photosynthesis

Photosystem II (PSII), a multi-subunit pigment-protein complex embedded in the thylakoid membrane of plants and cyanobacteria, utilizes water as an electron source for the light-driven reduction of quinones. A part of PSII often denoted as an oxygen-evolving complex (OEC) extracts four electrons (or reducing equivalents) and four protons from two water molecules; as a by-product of this water-oxidizing activity, dioxygen is released (Haumann & Junge, 1996; Nugent, 2001; Fig. 1). Essentially, all the molecular oxygen (O_2) in the earth's atmosphere has been produced by the light-driven water oxidation of PSII; the underlying chemistry seems to be unique and is, potentially, of technological interest. The center of the OEC comprises a tetranuclear manganese complex and, perhaps, one calcium as well as one chloride ion. The catalytic cycle of photosynthetic water oxidation involves four intermediate states denoted as *S* states (Fig. 1*b*). Mechanistically, photosynthetic water oxidation is not well understood. Structural information on the manganese complex in various states is needed to elucidate (at atomic level) how water is oxidized and how deleterious side-reactions are avoided.

2. Recent XAS results on the PSII manganese complex

2.1. Combination of LD-EXAFS and crystallographic information

The structural information carried by a single EXAFS spectrum is limited and frequently insufficient to develop a unique structural model of the metal site. To enhance the information content of XAS spectra, we are using a linear dichroism technique that requires the use of partially oriented samples and linearly polarized X-rays. Deposition of numerous layers of PSII membrane particles on a flat substrate material (*e.g.* a Kapton foil) leads to samples with a preferential orientation of the membrane normal in parallel to the sample's surface normal. Using these partially oriented samples for measurements at various angles, Θ_E, between the sample normal and electric-field vector of the polarized X-rays, determination of the linear dichroism in the X-ray spectra, which carries (limited) angle and orientation information (angle between absorber–backscatterer vector and membrane normal), becomes feasible (George *et al.*, 1989; Mukerji *et al.*, 1994; Dau *et al.*, 1995). Besides providing orientation information, dichroism data may facilitate the resolution of 'subshells' within a distinct coordination sphere that are not resolved by conventional EXAFS spectroscopy on isotropic samples. (We call this approach X-ray-absorption linear-dichroism spectroscopy, XALDS or, with respect to EXAFS spectra, LD-EXAFS. In the literature, the terms 'polarized EXAFS' or 'angle-dependent EXAFS' are frequently used.)

Because only imperfect unidirectional orientation is achievable, determination of the order characteristics (or 'mosaic spread') is mandatory for a quantitative analysis of XALDS data sets. Recently, we developed an approach to account correctly for the mosaic-spread characteristic and to carry out EXAFS simulations using the exact curved-wave EXAFS theory (Schiller *et al.*, 1998; Dittmer & Dau,

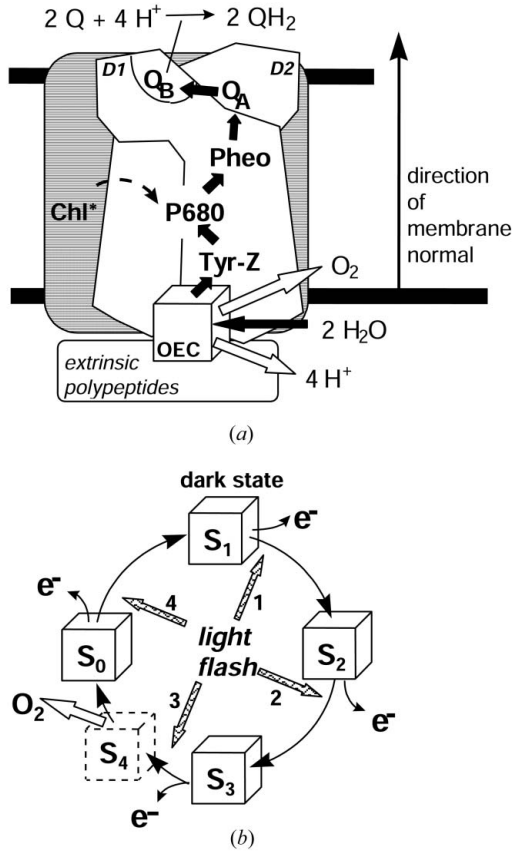

Figure 1
Scheme of the light-induced PSII reactions. Depicted is the arrangement of the relevant redox factors and the electron-transport paths (in *a*), the direction of the thylakoid membrane normal (in *a*) and the *S*-state cycling of the oxygen-evolving complex (OEC; in *b*). Following the absorption of a photon by the PSII pigments and ultra-fast excitation-energy transfer to a special set of chlorophylls called P680, electron transfer from P680 to a special pheophytin molecule is initiated. The primary electron donor P680 is re-reduced by a tyrosine residue (Tyr-161 of the D1 protein), and the resulting tyrosine radical delivers one oxidizing equivalent to the OEC. Driven by the one-electron oxidation that results from the absorption of a single photon, the OEC advances from the S_n state to the S_{n+1} state, where the subscripts give the number of oxidizing equivalents accumulated by the OEC. The most oxidized semi-stable state of the OEC is S_3; a further one-electron oxidation results in the formation of S_4, a hypothetical transition-state-like intermediate, which spontaneously relaxes to the S_0 state concurrently with the release of dioxygen. By application of saturating laser flashes of nanosecond duration (single-turnover flash), the OEC advances synchronously in the cycle by one *S* state of the cycle. Ideally, after four flashes the initial *S* state is reached a second time. However, on each flash a minority of PSII does not advance in the catalytic cycle (~10% 'misses'). Therefore, for applying a sequence of flashes, all signals related to the *S*-state cycle will exhibit a damped oscillation with a period of four flashes.

Table 1
Parameters obtained by a joint fit of k^3-weighted EXAFS spectra collected at four excitation angles (15, 35, 55, 75°) for the manganese complex in its S_1 state.

The value of N represents the 'EXAFS coordination number', meaning the average number of backscattering atoms 'seen' by each X-ray absorbing manganese; R is the mean distance between the atoms of the respective vector; σ, the Debye–Waller parameter, describes the distance spread due to static and dynamic disorder. θ_R is the average angle between the respective vector and the membrane normal. Numbers labeled * were not varied during the simulations but were fixed to reasonable values [based on preceding investigations by us and others; see Dau *et al.* (2001), Pospisil *et al.* (2001), Robblee *et al.* (2001)]. Technical details of the simulations: $E_0 = 6546$ eV; k-range, 2–12 Å; use of *FEFF*7 (Zhabinsky *et al.*, 1995); $S_0^2 = 0.85$; $I_{ord} = 0.5$ [order parameter as defined by Dittmer & Dau (1998); experimentally determined as described by Schiller *et al.* (1998)]; $R_F\{1.2–3.3$ Å$\} = 15\%$ [mean deviation between data and simulations in percent for EXAFS oscillations corresponding to distances ranging from 1.2 to 3.3 Å, see Meinke *et al.* (2000)]. The EXAFS data were collected at the bending-magnet XAS beamline of the EMBL outstation, Hamburg (HASYLAB/DESY).

Shell	Vector	N (per Mn)	R (Å)	$2\sigma^2$ (Å^2)	θ_R
I-*a*	Mn—O/N	3.5*	1.85	0.016	62°
I-*b*	Mn—O/N	2.0*	2.06	0.004	45°
II-*a*	Mn—Mn	0.5*	2.69	0.003*	60°
II-*b*	Mn—Mn	0.5*	2.73	0.003*	87°
III-*a*	Mn—Mn	0.5*	3.11	0.003*	85°
III-*b*	Mn—Ca	0.5*	3.31	0.003*	45°
III-*c*	Mn—O/N/*XX*	3.0*	3.65	0.019	54°

1998). This approach requires the simultaneous simulation (or 'fit') of EXAFS spectra collected at various excitation angles. Structural parameters obtained for the S_1 state by the joint fit of spectra collected at four distinct excitation angles are shown in Table 1.

Combination of structural information derived from EXAFS spectroscopy with insights into the chemical feasibility of potential structural motifs may facilitate the formulation of atomic resolution models. An example is the so-called 'Berkeley model' of the manganese complex in its S_1 state (see Sauer *et al.*, 1992; Yachandra *et al.*, 1993; Mukerji *et al.*, 1994; Dau *et al.*, 1995), which has already entered student textbooks (Shriver *et al.*, 1994; Lodish *et al.*, 2000). However, this prominent model is not uniquely implied by the data. Even on the basis of the refined LD-EXAFS results shown in Table 1 we cannot deduce a truly unique structural model. Absorber–backscatterer vectors exceeding a length of 4 Å are, at least presently, not observable. This means that (i) the structural information obtained by EXAFS does not cover the distance range required for discrimination between *e.g.* various isomeric forms of the same topological arrangement of the atoms in the core region of the Ca—Mn_4—(μ—O)$_n$-complex; (ii) in this system, identification of the ligating amino-acid residues by EXAFS spectroscopy seems to be difficult to achieve. With respect to both points, the less resolved (in terms of distance accuracy) but more global structural information obtainable by protein crystallography (Zouni *et al.*, 2001) may complement the LD-EXAFS data. At present, the resolution of the crystallographic data (~3.8 Å) is too low to identify the ligating amino-acid residues, but the electron-density map provides a shape or envelope for the electron density of the tetramanganese complex.

A first attempt to combine electron-density information and LD-EXAFS data is shown in Fig. 2. It should be noted that the model shown is still highly hypothetical, mostly owing to the relatively low resolution of the crystallographic data, the uncertainty (or noise) in the contour maps of electron densities and uncertainties with respect to the oxidation state of the manganese complex, which had been exposed to prolonged X-ray irradiation during the crystallographic data collection.

The modeling approach illustrated by Fig. 2 demonstrates the potential merits of combining low-resolution crystallographic data and the locally highly resolved information derived from EXAFS. More advanced approaches to combine EXAFS and crystallographic data are conceivable. Joint simulations of the electron-density maps (as obtained by protein crystallography) and EXAFS data may be advantageous.

2.2. Freeze-quench technique to capture semi-stable states

Typically, states of the enzyme with lifetimes exceeding tens of milliseconds at room temperature are stable at liquid nitrogen temperatures (~77 K) for several hours, days or weeks. The freeze-quench approach to investigating such semi-stable states by XAS involves (i) the initiation of a reaction at room temperature resulting in the fast formation of the semi-stable state ($\tau_{FORMATION} \ll \tau_{DECAY}$, $\tau_{DECAY} \simeq 100$ ms to 1 h), (ii) stabilization by rapid freezing (subsequent reactions are 'quenched' by the freezing) and (iii) XAS measurements at low temperatures (*e.g.* at 20 K). The freeze-quench approach has repeatedly been used in XAS studies (Bordas *et al.*, 1979; Strange *et al.*, 1993; Blackburn *et al.*, 2000). One method of initiating the reaction is the use of a stopped-flow setup. For example, the metalloenzyme and substrate are mixed and the rapidly formed semi-stable enzyme-substrate complex is investigated by XAS at low temperatures. In the case of PSII, however, the stopped-flow technique has never been used. Instead, transitions between states have been triggered by flashes of light.

It is possible to drive PSII through four intermediate states of its catalytic cycle by applying saturating flashes of short duration (1 ns–10 µs), the so-called 'single-turnover flashes'. An appropriate pretreatment results in PSII samples with an essentially exclusive

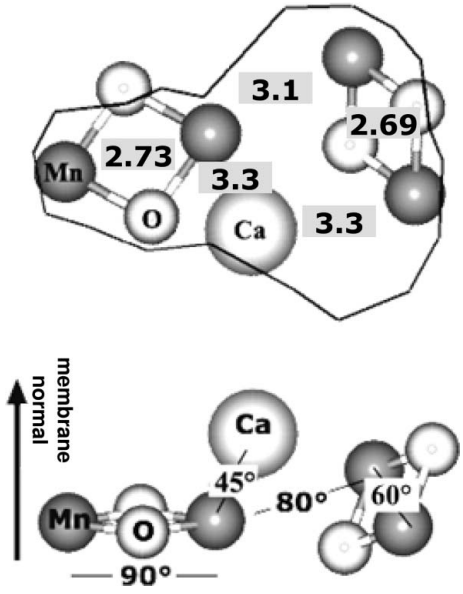

Figure 2
A tentative atomic resolution model of the structure of the Mn complex in the S_1 state (Haumann *et al.*, 2001). Top, viewed from lumen along the membrane normal; bottom, turned by 90° around the long axis. All of the manganese ligands (presumably five or six per manganese ion) are not shown; rather, the four Mn atoms, the bridging μ-oxo atoms and one Ca are depicted. The boundary of the electron density (solid line) was taken from Zouni *et al.* (2001). The Mn atoms separated by 3.1 Å are, presumably, bridged by a further mono-μ-oxo bridge. In the top scheme, some of the distances determined by EXAFS spectroscopy are given in Å; in the bottom scheme, the angles between absorber–backscatter vectors and the membrane normal are indicated. The position of the Ca ion is still highly speculative.

Table 2
Summary of simulation results obtained for the manganese complex in the four semi-stable states of its catalytic cycle (data collection at 20 K).

These results were obtained using the least complex simulation approach, which leads to acceptable simulations for distances smaller than 3 Å. Simulations of a more complex nature (including distances above 3 Å) suggest that, in the course of the S_2–S_3 transition, the increase in the number of 2.7 Å Mn—Mn vectors is coupled to the disappearance of the 3.1 Å Mn—Mn vector. The parameters labeled * were not varied in the course of the simulations. Upon the S_2–S_3 transition, not only the number but also the average angle (with respect to the membrane normal, last column) of the 2.7 Å Mn—Mn vectors is changed.

	N_1 (per Mn)	R_1 (Å)	$\pm\sigma_1$ (Å)	N_2 (per Mn)	R_2 (Å)	$\pm\sigma_2$ (Å)	Mn—Mn vectors (per Mn_4 complex)	$\langle\Theta_{2.7Å}\rangle$ (°)
S_1	6*	1.87	0.13	1.1	2.71	0.04	2 × 2.7 Å	> 70
S_2	6*	1.86	0.11	0.9	2.71	0.03	2 × 2.7 Å	> 70
S_3	6*	1.85	0.09	1.6	2.74	0.04	3 × 2.7 Å (or 2 × 2.7 Å plus 1 × 2.8 Å)	≃ 60
S_0	5*	1.88	0.11	1.0	2.75	0.05	1 × 2.7 Å plus 1 × 2.8 Å	> 70
	1*	2.2*	0.02*					

population of the S_1 state (see *e.g.* Iuzzolino *et al.*, 1998). By applying one laser flash, the S_2 state is populated. The second flash results in the predominant population of the S_3 state. The third flash triggers the oxygen-evolution transition resulting in preferential population of the S_0 state. The fourth flash closes the cycle by forming the S_1 state in the majority of PSII. The flash approach does not allow the preparation of pure *S* states; only preferential population of *S* states is achievable. Therefore, it is necessary to correct for undesired minority contributions of *S* states. This can be done by calculating pure *S*-state spectra based on the measured spectra and the estimated *S*-state population distribution [*e.g.* estimated based on the quaternary oscillations of the magnitude of an EPR-signal present only in the S_2 state (Roelofs *et al.*, 1996; Iuzzolino *et al.*, 1998)]. Using such a deconvolution to obtain EXAFS spectra of the pure *S* states, we obtained the results summarized in Fig. 3 (Fourier-transformed spectra) and Table 2 (simulation results) (Dau *et al.*, 1998, 2001). A hypothetical 'structural cycle' of the water-oxidizing manganese complex as derived from the EXAFS results is shown in Fig. 4. Further details and the implications for the mechanism of water oxidation are discussed elsewhere (Dau *et al.*, 2001).

In summary, using a freeze-quench approach it has been possible to obtain structural information for four intermediate states of the *S*-state cycle of PSII. The catalytic cycle involves distinct structural changes in the core of the metal complex, which are detectable by EXAFS spectroscopy. The observed changes are clearly important

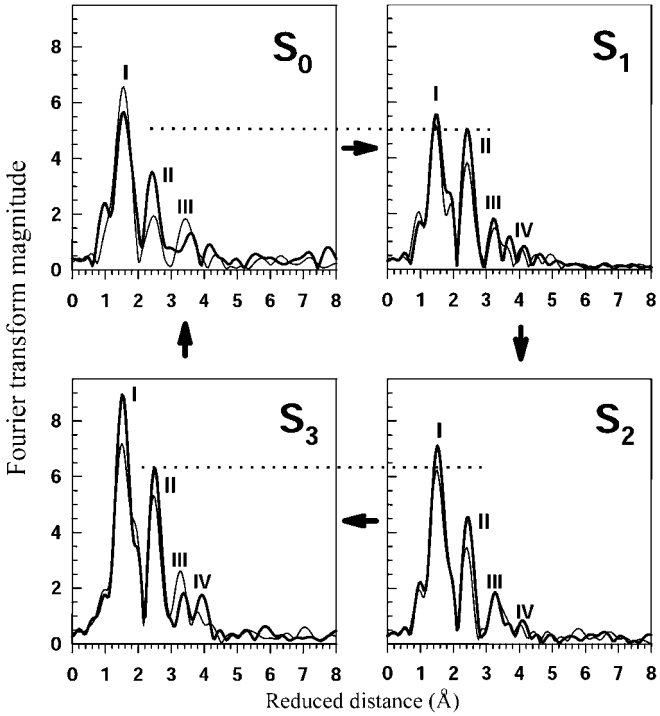

Figure 3
Fourier-transformed EXAFS spectra for pure *S* states collected at 20 K. The spectra shown were collected on unidirectionally oriented PSII-membrane particles at the 'magic angle' of 55° (thick line) and at 15° (thin line) [Dau *et al.* (1998); data collection at the XAS beamline of the EMBL outstation, Hamburg, at DESY]. The internuclear distance between the X-ray-absorbing Mn atom and the backscattering atoms is 0.3–0.5 Å larger than the indicated reduced distance because of a linear *k*-dependence of the phase of the complex EXAFS-backscattering amplitudes.

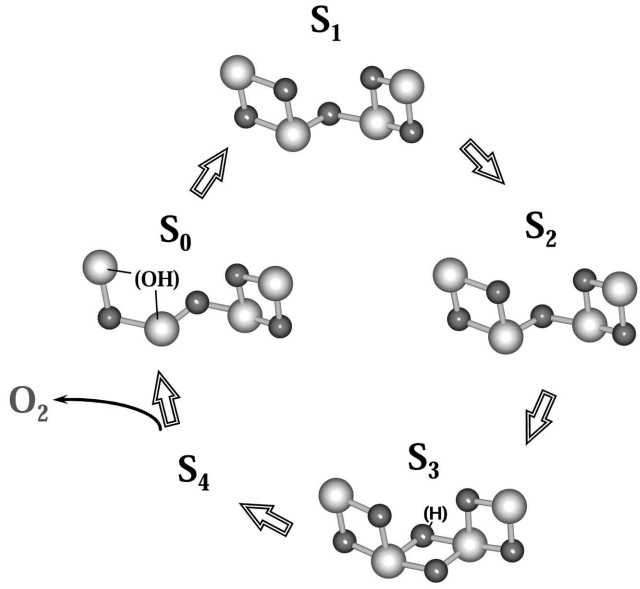

Figure 4
Proposed structural cycle for the core of the Photosystem II manganese complex. Only the four manganese ions and the bridging oxides are depicted. In the S_1 state (the dark state) and in the S_2 state, two di-μ-oxo bridged binuclear manganese units (Mn—Mn distance ∼2.7 Å) are connected by a mono-μ-oxo bridge (Mn—Mn distance 3.1 Å). The S_0 structure differs from the S_1 structure, presumably because of the presence of a singly protonated di-μ-oxo bridge (Mn—Mn distance ∼2.8 Å). In the S_3 state the four manganese ions seem to be connected by three di-μ-oxo bridges (three Mn—Mn vectors of ∼2.7 Å); a single μ-oxo bridge might be protonated. Thus, upon the S_0–S_1 transition a bridging oxide is deprotonated, whereas the S_2–S_3 transition involves the deprotonation of a terminal oxo ligand and the formation of a new μ-oxo bridge, presumably assisted by the transformation of five-coordinated Mn(III) to six-coordinated Mn(IV) (as discussed by Dau *et al.*, 2001). The changes occurring upon the manganese-oxidizing transitions of the cycle are, necessarily, reversed during the oxygen-evolving and manganese-reducing S_3–(S_4)–S_0 transition. Putative consequences for mechanistic models of photosynthetic water oxidation are discussed elsewhere (Dau *et al.*, 2001).

for the formulation and evaluation of mechanistic models (see Dau *et al.*, 2001).

2.3. Time-resolved BioXAS using a freeze-quench approach

Freeze-quench techniques can also be employed for time-resolved investigations. By freezing samples at discrete times after the initiating event, the time-evolution of the XAS-detectable structural changes can be monitored. The time resolution of the freeze-quench approach is limited by the freezing time (> 10 ms); to observe faster processes alternative approaches are needed (see §2.4). A variety of conceivable events can 'trigger' the reaction, *e.g.* rapid mixing of the enzyme and its substrate, pH-jumps, a sudden change in the redox potential, a light pulse (see §2.2), and temperature jumps. In the following, we discuss the first time-resolved freeze-quench investigation involving XAS on the PSII manganese complex (Pospisil *et al.*, 2001, 2002). In this particular case, the processes of interest are conveniently slow. The trigger event is a stepwise increase in temperature (temperature jump), which initiates the stepwise disassembly of the tetramanganese complex of PSII.

The PSII membrane samples were suddenly exposed to a temperature of 320 K; and the processes initiated by this temperature jump were stopped by rapid cooling after heating times ranging from 0 to 180 min. This protocol facilitates the detailed analysis of the time course (or kinetics) of the heat-induced changes at the Mn complex by oxygen polarography (not shown), EPR spectroscopy (not shown) and X-ray absorption spectroscopy (Fig. 5*a*).

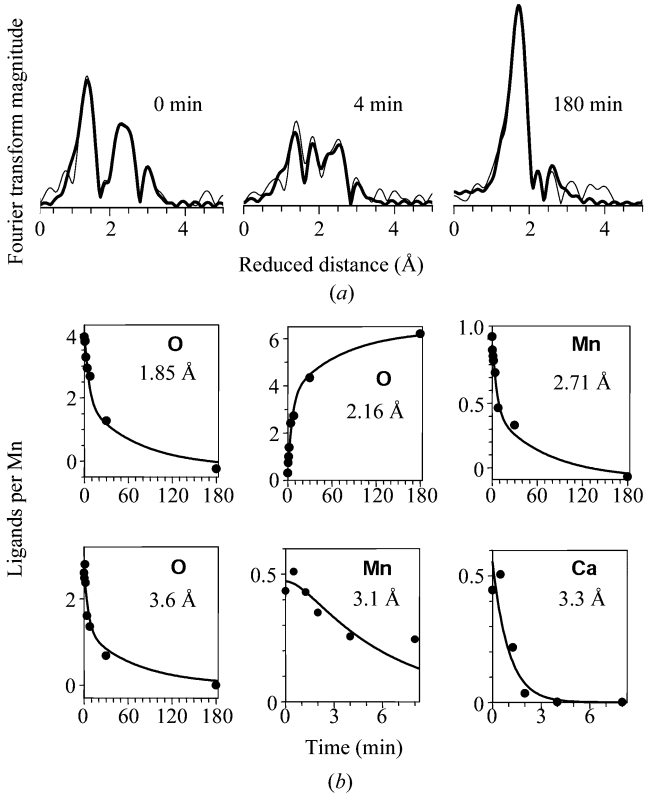

Figure 5
Temporal changes of the EXAFS in response to a temperature jump (at $t = 0$). (*a*) Fourier transforms of k^3-weighted EXAFS oscillations of the Mn complex of PSII multilayers exposed to 320 K for 0, 4 and 180 min. Thin lines, experimental data; thick lines, simulations. (*b*) Time courses of the coordination numbers of six shells of backscatterers resulting from a joint fit of eight EXAFS spectra. The points are the coordination numbers as determined by the joint fit; the solid lines were calculated based on the consecutive reaction shown in Fig. 6. The good agreement between calculated and experimentally determined coordination numbers confirms the validity of the reaction scheme used (Pospisil *et al.*, 2002).

Eight EXAFS spectra, representing eight different heating times, were fitted simultaneously by parameter variations and minimization of a common error sum (R_F). The same set of distances and Debye–Waller parameters was used for all eight spectra, whereas all the coordination numbers were allowed to vary independently. The joint simulation of the eight spectra using common distance and Debye–Waller parameters facilitates the resolution of six distinct shells of ligand atoms. In Fig. 5(*b*), the resulting Mn—ligand distance and the time course of the respective coordination number are shown for each of the six shells of backscattering atoms. The low R_F value (around 11%) confirms the high quality of the fits. Other simulation approaches (higher or lower number of ligand shells) yielded significantly higher R_F values or erratic time courses of the coordination numbers.

The next step in the analysis of the time-series of EXAFS spectra was the application of an appropriate kinetic model. Assuming that a consecutive reaction scheme involving four discrete states and three first-order rate constants describing the transitions between these states is sufficiently complex (Fig. 5), we simulated the time courses of the six coordination numbers and the time course of 'supplementary' signals [the activity loss, the occurrence of $Mn(H_2O)_6^{2+}$ as detected by EPR spectroscopy and the X-ray edge position]. This simulation involved the simultaneous fit of the nine time courses [$6 \times N_i$, activity, amount of $Mn(H_2O)_6^{2+}$, edge position] using the same set of rate constants (k_1, k_2 and k_3) for each time course. These simulations provide rate-constant values, and the coordination numbers associated with each of the four 'pure' states can also be obtained.

In any kinetic BioXAS investigation, at most times a mixture of different states is present and the spectra constitute a linear superposition of the spectra of the individual states. At first glance, this constitutes a major problem, because the resulting complexity of the EXAFS spectra hampers a meaningful simulation of the individual spectra (too many backscatterer shells involved). We dealt with that problem by using a specific joint-fit approach (or 'global analysis'), which is based on the assumption that a single set of absorber–backscatterer distances can facilitate an adequate description of all the collected EXAFS spectra. Using this joint-fit approach, the time dependence of the (apparent) coordination numbers, $N_i(t)$, was obtained (Fig. 6). We found that avoidance of erratic time courses of the coordination numbers provides a useful criterion for the choice of an appropriate number of backscatterer shells. Guided by the time courses, a kinetic model (or scheme) was constructed where the rate-limiting steps are described by first-order rate constants. On the basis of this kinetic model, the rate-constant values and structural models (or at least structural information) for the involved intermediates

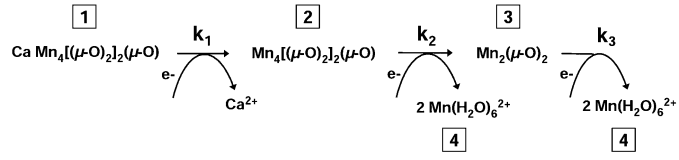

Figure 6
A kinetic scheme for the stepwise reduction and disassembly of the Mn complex in response to a temperature jump. The rate constants as determined by the joint analysis of nine time courses {six coordination numbers, $N_i(t)$; activity, $R(t)$; amount of $Mn(H_2O)_6^{2+}$, $[Mn^{2+}](t)$; X-ray edge position, $E_{EDGE}(t)$} are $k_1 = 1\ min^{-1}$, $k_2 = 0.18\ min^{-1}$ and $k_3 = 0.014\ min^{-1}$ (Pospisil *et al.*, 2001, 2002).

have been obtained. This means that the deconvolution of the structural information carried by the EXAFS spectra has been obtained by exploiting the kinetic information provided by the time-resolved experiment. In the future, even more advanced data-evaluation approaches might be profitable; *e.g.* joint simulations of a series of spectra using the same set of distances for all spectra but using a multi-exponential model for the time dependence of the apparent coordination numbers.

In summary, the freeze-quench approach used here involves measurements of spectra for a (limited) number of sampling times; it can facilitate the time-resolved observation of structural changes occurring in the course of a reaction sequence. In the BioXAS study reviewed above, the required time resolution was low, but this investigation demonstrates very well the principal problems and benefits of time-resolved BioXAS. The following has been achieved: (i) determination of the reaction sequence (construction of a kinetic model), (ii) determination of the rate-constant values of the rate-limiting steps, (iii) structural characterization of the initial, two intermediate and one final states.

2.4. Room-temperature experiments and 'real-time' BioXAS

The PSII manganese complex has been investigated by numerous EPR measurements of signals stemming from the PSII manganese complex, which are detectable only at low temperatures. Such investigations revealed a complex cryochemistry (Britt, 1996; Nugent, 2001), but the relevance of the obtained results for catalysis at room temperature is not beyond doubt. It is an important methodological advantage that XAS on metalloproteins is not limited to measurements at low temperature. In principle, the enzyme can be studied under quasi-native conditions at temperatures where efficient catalysis occurs.

The rate of so-called radiation damage caused by the X-ray irradiation is significantly accelerated at higher temperatures. At room temperature, using a high-flux undulator beamline, X-ray irradiation may influence structure and metal oxidation state significantly in less than a minute. Thus, room-temperature measurements on metalloproteins require particularly careful assessment of radiation-induced modifications of the investigated metal site and, subsequently, choice of an appropriate experimental strategy to avoid any significant influence of radiation effects on experimental results. Recently, we could demonstrate that optimized samples and rapid-scan capabilities of a modern synchrotron source render high-quality XAS investigations of room-temperature structure and oxidation state of the oxygen-evolving PSII manganese complex feasible (Meinke *et al.*, 2000; Haumann *et al.*, 2001, 2002). The increase of Debye–Waller parameters (σ) upon temperature increase results in more damped EXAFS oscillations, but the amount of extractable structural information is found not to be significantly lower at room temperature. Room-temperature XAS investigations open a new road to gaining insights into the structure–function relationships involved in photosynthetic water oxidation. Structural investigations under defined (*e.g.* with respect to pH) and 'almost native' conditions become viable; the ambiguity with respect to the relevance of low-temperature results is avoidable. In addition, the capability to investigate the metalloenzyme at its 'working temperature' is the prerequisite for time-resolved XAS investigations aiming at observation of structural changes in 'real time' (without using a freeze-quench approach).

Measurements at room temperature obviously exclude the use of a freeze-quench approach. To investigate the *S*-state transition of the PSII manganese complex at room temperature we have used an alternative approach. To drive the manganese complex through its catalytic cycle, the biological samples were illuminated within the experimental hutch of the beamline (ID 26, ESRF, Grenoble) by nanosecond laser flashes (see Fig. 7). For X-ray measurements two different protocols were used: (i) during illumination with a sequence of laser flashes, time courses of the fluorescence intensity were monitored for excitation at fixed X-ray excitation energy (in the region of the Mn *K*-edge); (ii) immediately after application of n laser flashes (n = 0, 1, 2, 3), spectra were rapidly collected (rapid scanning of the X-ray excitation energy).

By rapid scanning of the crystal monochromator, it is possible to collect spectra of the X-ray edge in only ∼2 s. The achieved signal-to-noise ratio (for the PSII samples) was sufficient to determine the edge position based on a single scan with a precision of better than 0.2 eV (Meinke *et al.*, 2000). The rapid-scan mode used for collection of EXAFS spectra involves simultaneous scanning of the monochromator and undulator gap resulting in scan periods for a complete EXAFS spectrum (6400–7100 eV) of only 9 s. [For further experimental details see Gauthier *et al.* (1999), Signorato *et al.* (1999), Solé *et al.* (1999), Meinke *et al.* (2000).] For two reasons, the rapid-scan capabilities of the beamline used (ID26, ESRF, Grenoble) have been crucial for the success of the laser-flash experiments. Firstly, the intermediate states of the catalytic cycle populated by the laser flashes decay with half-lifetimes ranging from minutes to hours. This means that, to avoid any influence of changes in the *S*-state population distribution, the XAS measurements need to be completed in less than ∼30 s after the end of a flash sequence. Secondly, for the chosen experimental conditions, X-ray exposure times exceeding ∼15 s may lead to an X-ray photoreduction of the manganese complex in a non-negligible fraction of PSII.

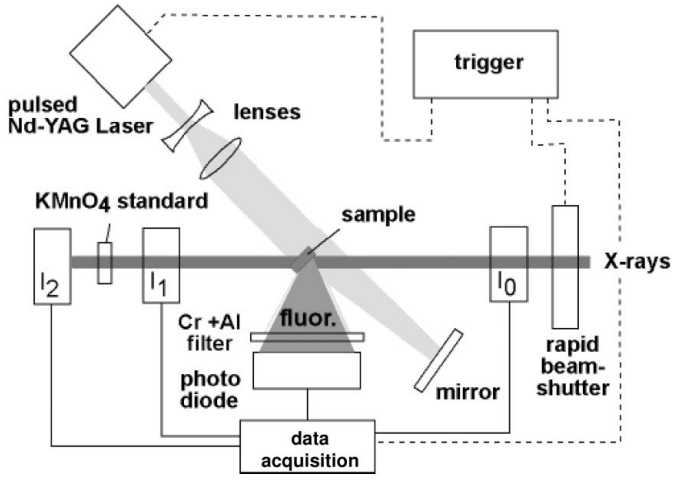

Figure 7
Experimental setup to drive the PSII through its catalytic cycle by applying nanosecond laser pulses at the beamline. Laser-flash excitation of the samples was performed at the beamline ID26 (ESRF, Grenoble) using a frequency-doubled Q-switched Nd-YAG laser (Quantel Brilliant, FWHM 5 ns, 532 nm, *ca.* 150 mJ per flash). The laser beam was widened by lenses to a spot size of *ca.* 20 × 8 mm. Half of the spot illuminated the front-side of the sample directly. The other half was reflected by a mirror to the back-side of the sample. This setup ensured simultaneous and homogenous illumination of the sample from both sides. A chromium filter and a thin aluminium foil in front of the photodiode suppressed scattered X-rays and laser light, respectively. The absorption spectrum of $KMnO_4$ was measured to facilitate a precise energy calibration. To minimize X-ray exposure times (radiation damage), a rapid beam shutter was used that opened only immediately before the start of the X-ray measurements. The rapid beam shutter, laser flashes, and data acquisition were synchronized using appropriate trigger electronics.

Owing to the oxidation-state changes of the PSII manganese complex, the position of the X-ray edge changes in the course of the *S*-state cycle. By using an excitation energy in the rising part of the edge spectrum, we can monitor the pronounced absorption changes that result from a shift of the edge spectrum. Therefore, the time course of the X-ray fluorescence intensity measured at fixed excitation energy reflects the cyclic progression of the PSII manganese complex through its catalytic cycle and facilitates determination of the *S*-state composition obtained by applying a given number of flashes (Fig. 8*a*). By collecting time courses at several excitation energies, it is also possible to determine the changes in the shape of the X-ray edge spectra associated with each *S*-state transition (not shown).

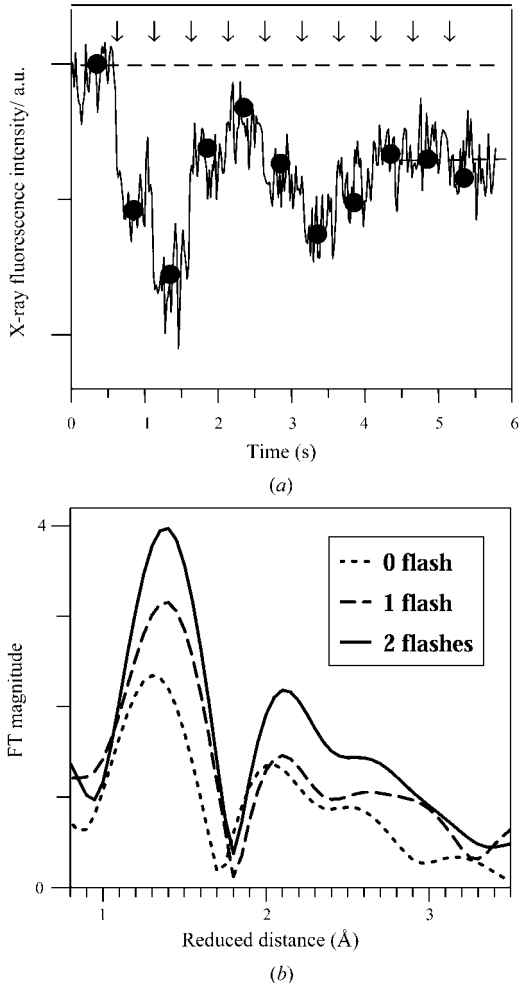

Figure 8
Room-temperature results of the laser-induced changes in the XAFS of the PSII manganese complex. The experimental setup depicted in Fig. 7 was used. (*a*) Time course of the X-ray fluorescence intensity at 6551.5 eV of the manganese complex (edge region) driven repeatedly through its catalytic cycle by a sequence of ten laser flashes (at 291 K). The quaternary oscillations verify the cyclic progression of the manganese complex through the *S*-state cycle. The damping of the quarternary oscillation is well reproduced using an initial population of S_1 of 100% and 15% of 'misses' (closed circles represent the simulated values). From these numbers, we estimate the yields of S_1, S_2 and S_3 after flashes 0, 1 and 2 to be 100, 85 and 72%, respectively. (*b*) Fourier transforms of k^3-weighted EXAFS spectra collected at room temperature for predominant population of the S_1, S_2 and S_3 states. Dark adaptation resulted in exclusive population of the S_1 state; by applying one and two laser flashes the S_2 and S_3 states, respectively, were populated. Immediately after the flash illumination a rapid EXAFS scan lasting for not more than 10 s was started (simultaneous scans of monochromator and undulator gap, beamline ID26, ESRF, Grenoble).

We collected EXAFS spectra within 10 s after the application of zero (100% of PSII in the S_1 state), one (~85% of PSII in the S_2 state) and two laser flashes (~72% of PSII in the S_3 state). Each of the oxidizing *S*-state transitions is associated with an increase in the magnitude of the first Fourier peak (Fig. 8*b*). Particularly interesting, however, is the increase in the second Fourier peak induced by the second laser flash. This increase suggests that at room temperature the S_2–S_3 transition is associated with the formation of an additional μ-oxo bridge (Haumann *et al.*, 2001, 2002).

In summary, time courses (at fixed excitation energy, Fig. 8*a*) and spectra for different intermediate states of the catalytic cycle (Fig. 8*b*) were collected at room temperature. Thus, advancement through the catalytic cycle as well as changes in room-temperature structure of the non-crystalline sample have been monitored by BioXAS. The reviewed experiments demonstrate the feasibility and potential of room-temperature BioXAS, and they constitute an important first step towards room-temperature experiments that are more advanced.

In the time-resolved experiment described in §2.3, we followed directly the time course of the reaction. In the room-temperature experiments, the kinetics of the *S*-state transitions induced by the laser pulse are not resolved. These transitions occur in the micro- and millisecond range. In principle, the experiment of Fig. 8(*a*) should also allow for an analysis of the transition kinetics themselves. By performing the experiment for several fixed energies, it may become possible to follow the changes in the spectra with high time resolution. At present, the data acquisition system and, in particular, signal-to-noise problems impede investigations at higher time resolution. Thus, further technical improvements are required to make meaningful BioXAS experiments at high time resolution feasible. Using a high-flux undulator beamline, it should be possible to carry out BioXAS experiments with millisecond time resolution in the near future.

In this review, we have not explicitly included another type of BioXAS experiment on catalysis at metal sites because, at present, this promising line has not been pursued in the context of investigations on the PSII manganese complex. Investigations of states populated in the course of 'titration curves' (pH, redox potential, substrate concentration) are envisioned. Such kinetic investigations (in biochemistry, substrate titrations are referred to as 'enzyme kinetics') require the collection of sets of XAFS spectra for various values of the titration parameter. With respect to the benefits of such investigations and the need for advanced data-evaluation strategies, the titration experiment closely resembles the time-resolved experiment discussed in §2.3. However, in a pH or redox titration the BioXAS measurement should be performed, preferentially, at room temperature to avoid the potential effect of changes in pH values or redox potential upon freezing.

3. Tasks and perspectives

The experiments reviewed above demonstrate the general feasibility of BioXAS investigations to 'watch' catalysis at protein-bound metal centers. These experiments have become possible owing to the impressive progress made in the performance characteristics of synchrotron radiation sources and at the experimental stations dedicated to the study of (ultra-dilute) biological samples. However, the reviewed experiments represent only the first steps. Further methodological developments are required to make the full potential of the BioXAS approach accessible.

3.1. Improvements of methodology at the synchrotron radiation sources

It is self-evident that any time-resolved or titration-type experiment requires the collection of a full set of high-quality spectra. The collection of the eight spectra shown in Fig. 3 requires about four weeks of beam time at a typical bending-magnet beamline. To progress with these types of studies (*e.g.* to investigate the structural changes occurring in the catalytic cycle for several mutated enzymes), low-temperature BioXAS experiments with an increased throughput are desirable.

The major impediment with respect to more advanced time-resolved BioXAS experiments at room temperature is the achievable signal-to-noise ratio. Conceivable improvements are an increase in the number of incident X-ray photons per second (and not per area) and, to minimize radiation damage, a moderate increase in the irradiated area (to about 1×2 mm); improved fluorescence detection schemes; optimized geometry (increased fluorescence signal for grazing-incidence excitation); and a higher throughput by fully automated sample changing.

The room-temperature experiments of the type shown in Fig. 8(*b*) require rapid-scan capabilities to cope with the decay of the investigated state. In principle, even shorter scan times can be achieved [*e.g.* Piezo-QEXAFS (Lützenkirchen-Hecht *et al.*, 2001); dispersive optics and sequential fluorescence data acquisition (Pascarelli *et al.*, 1999)].

3.2. State population and data analysis in the future

In the case of PSII, using an appropriate laser-flash protocol, each of the four semi-stable states of the catalytic cycle can be preferentially populated. For processes that are not directly excitable by light, alternative approaches to 'trigger' the reaction sequence are needed. A variety of methods need to be tested with respect to their compatibility with BioXAS experiments (stopped-flow and continuous-flow methods, temperature jumps or pulses, pressure jumps or pulses, sudden application of strong electric fields, sudden change in the potential of a redox electrode *etc.*). For experiments at high time resolution, the initiation by laser flashes seems to be the most practicable way. It is foreseeable that the continuously growing array of phototriggers will become increasingly important. Examples of such phototriggers are caged compounds that are released upon illumination with an intense flash of light (*e.g.* ATP, Ca^{2+}, protons) and the flash-photolysis of CO successfully employed in XAS studies of myoglobin (Teng *et al.*, 1987; Ascone *et al.*, 1993).

If the structure of the metal site in its ground or resting state is known, it will be significantly easier to deduce unique structural models for intermediate states of the catalytic cycle. To derive highly resolved structural models of the metal site in its resting state, the combination of BioXAS data analysis with structural information obtained by protein crystallography or by molecular modeling is likely to become increasingly important (see §2.1).

It is likely that the first BioXAS investigations with high time resolution will be restricted to the XANES region of the spectrum. Therefore, the development of methods to deduce structural information from XANES spectra is of high interest.

The analysis of kinetic data sets (time-resolved data or titration curves) requires the use of data evaluation approaches that involve some kind of 'global analysis' of a set of spectra. In §2.3, a first step towards a global data analysis of time-resolved data is presented; more advanced approaches are likely to be profitable.

We thank Drs Hilmar Schiller, Jens Dittmer, Lucia Iuzzolino and Wolfgang Dörner for collection and analysis of the BioXAS data reviewed in §§2.1 and 2.2. These experiments have been carried out in cooperation with Dr Wolfram Meyer-Klaucke at the XAS beamline of the EMBL outstation, Hamburg (HASYLAB/DESY). We thank him and the staff of the EMBL outstation for support. The experiments discussed in §2.3 were initiated and carried out by Dr Pavel Pospisil (now at Harvard University, Boston, USA). The experiments reviewed in §§2.3 and 2.4 were performed in collaboration with Drs Armando Solé and Thomas Neisius at beamline ID26 of the ESRF; Carsten Meinke, Markus Grabolle, Martin Werthammer, Peter Liebisch and Claudia Müller contributed significantly to data collection and analysis. We thank all of them and the involved staff at the ESRF. Financial support by the German BMBF (program Erforschung Kondensierter Materie, grant No. 05KS1KEA/6) and the Deutsche Forschungsgemeinschaft (SFB 498, TP C6) is gratefully acknowledged.

References

Ankudinov, A., Ravel, B., Rehr, J. & Conradson, S. (2001). *Phys. Rev. B*, **58**, 7565–7576.
Armstrong, W. H. (1992). *Manganese Redox Enzymes*, edited by V. L. Pecoraro, pp. 261–286. New York: VCH.
Ascone, I., Longo, A., Dexpert, H., Ciriolo, M. R., Rotilio, G. & Desideri, A. (1993). *FEBS Lett.* **322**, 165–167.
Blackburn, N. J., Rhames, F. C., Ralle, M. & Jaron, S. (2000). *J. Biol. Inorg. Chem.* **5**, 341–353.
Bordas, J., Bray, R. C., Garner, C. D., Gutteridge, S. & Hasnain, S. S. (1979). *J. Inorg. Biochem.* **11**, 181–186.
Bossek, U., Hummel, H., Weyhermüller, T., Wieghardt, K., Russel, S., van der Wolf, L. & Kolb, W. (1996). *Angew. Chem.* **108**, 1653–1656.
Britt, R. D. (1996). *Oxygenic Photosynthesis: The Light Reactions*, edited by D. R. Ort & C. F. Yocum, pp. 137–164. Dordrecht: Kluwer Academic Publishers.
Cowan, J. A. (1996). *Inorganic Biochemistry: An Introduction.* New York: John Wiley and Sons.
Cramer, S. P., Wang, H., Bryant, C., Legros, M., Horne, C., Patel, D., Ralston, C. & Wang, X. (1998). *Am. Chem. Soc. Symp. Ser.* **692**, 154–178.
Dau, H., Andrews, J. C., Roelofs, T. A., Latimer, M. J., Liang, W., Yachandra, V. K., Sauer, K. & Klein, M. P. (1995). *Biochemistry*, **34**, 5274–5287.
Dau, H., Dittmer, J., Epple, M., Hanss, J., Kiss, E., Rehder, D., Schultze, C. & Vilter, H. (1999). *FEBS Lett.* **457**, 237–240.
Dau, H., Iuzzolino, L. & Dittmer, J. (2001). *Biochim. Biophys. Acta*, **1503**, 24–39.
Dau, H., Iuzzolino, L., Dittmer, J., Dörner, W. & Meyer-Klaucke, W. (1998). *Photosynthesis: Mechanism and Effects*, edited by G. Garab, Vol. II, pp. 1327–1330. Dordrecht: Kluwer Academic Publishers.
DeBeer George, S., Metz, M., Szilagyi, R. K., Wang, H., Cramer, S. P., Lu, Y., Tolman, W. B., Hedman, B., Hodgson, K. O. & Solomon, E. I. (2001). *J. Am. Chem. Soc.* **123**, 5757–5767.
Dittmer, J. & Dau, H. (1998). *J. Phys. Chem. B*, **102**, 8196–8200.
Dittmer, J., Iuzzolino, L., Dörner, W., Nolting, H.-F., Meyer-Klaucke, W. & Dau, H. (1998). *Photosynthesis: Mechanism and Effects*, edited by G. Garab, Vol. II, pp. 1339–1342. Dordrecht: Kluwer Academic Publishers.
Filliponi, A., Di Cicco, T. A., Tyson, T. A. & Natoli, C. R. (1991). *Solid State Commun.* **78**, 265.
Gauthier, C., Solé, V. A., Signorato, R., Goulon, J. & Moguiline, E. J. (1999). *J. Synchrotron Rad.* **6**, 164–166.
George, G. N., Prince, R. C. & Cramer, S. P. (1989). *Science*, **234**, 789–791.
Gurman, S. I., Binsted, N. & Ross, I. (1984). *J. Phys. C*, **17**, 143–151.
Haumann, M., Grabolle, M., Neisius, T. & Dau, H. (2002). *FEBS Lett.* **512**, 116–120.
Haumann, M., Grabolle, M., Werthammer, M., Iuzzolino, L., Dittmer, J., Meyer-Klaucke, W., Neisius, T. & Dau, H. (2001). *Proceedings of the Twelth International Congress on Photosynthesis.* Brisbane, Australia: CIRSO. http://www.publish.csiro.au/ps2001/cf/home/index.cfm.
Haumann, M. & Junge, W. (1996). *Oxygenic Photosynthesis: The Light Reactions*, edited by R. D. Ort & C. F. Yocum, pp. 165–192. Dordrecht: Kluwer Academic Publishers.
Hill, H. A. O., Sadler, P. J. & Thomson, A. J. (1999). *Metal Sites in Proteins and Models.* Berlin: Springer.

Iuzzolino, L., Dittmer, J., Dörner, W., Meyer-Klaucke, W. & Dau, H. (1998). *Biochemistry*, **37**, 17112–17119.
Iwata, S., Ostermeier, C., Ludwig, B. & Michel, H. (1995) *Nature (London)*, **376**, 660–669.
Kirby, J. A., Goodin, D. B., Wydrzynski, T., Robertson, A. S. & Klein M. P. (1981). *J. Am. Chem. Soc.* **103**, 5537–5542.
Kirby, J. A., Robertson, A. S., Smith, J. P., Thompson, A. C., Cooper, S. R. & Klein, M. P. (1981). *J. Am. Chem. Soc.* **103**, 5529–5537.
Larson, E. J., Riggs, P. J., Penner-Hahn, J. E. & Pecoraro, V. L. (1992). *J. Chem. Soc. Chem. Commun.* pp. 102–103.
Lippard, S. J. & Berg, J. M. (1994). *Principles of Bioinorganic Chemistry*. Sausalito: University Science Books.
Lodish, H., Berk, A., Zipursky, S. L., Matsudaira, P., Baltimore, D. & Darnel, J. (2000). *Molecular Cell Biology*. New York: Freeman.
Lützenkirchen-Hecht, D., Grundmann, S. & Frahm, R. (2001). *J. Synchrotron Rad.* **8**, 6–9.
MacLachlan, D. J., Hallahan, B. J., Ruffle, S. V., Nugent, J. H. A., Evans, M. C. W., Strange, R. W. & Hasnain, S. S. (1992). *Biochem. J.* **285**, 569–576.
Meinke, C., Solé, V. A., Pospisil, P. & Dau, H. (2000). *Biochemistry*, **39**, 7033–7040.
Mukerji, I., Andrews, J. C., DeRose, V. J., Latimer, M. J., Yachandra, V. K., Sauer, K. & Klein, M. P. (1994). *Biochemistry*, **33**, 9712–9721.
Nugent, J. (2001). *Biochim. Biophys. Acta*, **1503**, 1–259.
Pascarelli, S., Neisius, T. & De Panfilis, S. (1999). *J. Synchrotron Rad.* **6**, 1044–1050.
Peariso, K., Zhou, Z. S., Smith, A. E., Matthews, R. G. & Penner-Hahn, J. E. (2001). *Biochemistry*, **40**, 987–993.
Pecoraro, V. L. (1992). *Manganese Redox Enzymes*, edited by V. L. Pecoraro, pp. 197–231. Weinheim, Germany: VCH.
Penner-Hahn, J. E. (1999). *Metal Sites in Proteins and Models. Redox Centres*, edited by H. A. O. Hill, P. J. Sadler & A. J. Thomson, pp. 1–36. Heidelberg: Springer Verlag.
Penner-Hahn, J. E., Fronko, R. M., Pecoraro, V. L., Yocum, C. F., Betts, S. D. & Bowlby, N. R. (1990). *J. Am. Chem. Soc.* **112**, 2549–2557.
Pospisil, P., Haumann, M., Dittmer, J., Sole, A. & Dau, H. (2001). *Proceedings of the Twelth International Congress on Photosynthesis.* Brisbane: CIRSO. http://www.publish.csiro.au/ps2001/cf/home/index.cfm.
Pospisil, P., Haumann, M., Dittmer, J., Sole, A. V. & Dau, H. (2002). *Biophys. J.* In the press.
Rehr, J. J., Mustre de Leon, J., Zabinsky, S. I. & Albers, R. C. (1991). *J. Am. Chem. Soc.* **113**, 5135–5140.
Robblee, J. H., Cinco, R. M. & Yachandra, V. K. (2001). *Biochim. Biophys. Acta*, **1503**, 7–23.
Roelofs, T. A., Liang, W., Latimer, M. J., Cinco, R. M., Rompel, A., Andrews, J. C., Sauer, K., Yachandra, V. K. & Klein, M. P. (1996). *Proc. Natl Acad. Sci. USA*, **93**, 3335–3340.
Sauer, K. (1995). Editor. *Biochemical Spectroscopy, Methods in Enzymology*, Vol. 246. New York: Academic Press.
Sauer, K., Yachandra, V. K., Britt, R. D. & Klein, M. (1992). *Manganese Redox Enzymes*, edited by V. L. Pecoraro, pp. 85–103. New York: VCH.
Schiller, H., Dittmer, J., Iuzzolino, L., Dörner, W., Meyer-Klaucke, W., Solé, V. A. & Dau, H. (1998). *Biochemistry*, **37**, 7340–7350.
Scott, R. A. (2000). *Physical Methods in Bioinorganic Chemistry – Spectroscopy and Magnetism*, edited by L. Que Jr, pp. 465–504. Sausalito: University Science Books.
Shriver, D. F., Atkins, P. W. & Langford, C. H. (1994). *Inorganic Chemistry*. Oxford University Press.
Signorato, R., Solé, V. A. & Gauthier, C. (1999). *J. Synchrotron Rad.* **6**, 176–178.
Solé, V. A., Gauthier, C., Goulon, J. & Natali, F. (1999). *J. Synchrotron Rad.* **6**, 174–175.
Strange, R., Morante, S., Stefanini, S., Chiancone, E. & Desideri, A. (1993). *Biochim. Biophys. Acta*, **1164**, 331–334.
Teng, T. Y., Huang, H. W. & Olah, G. A. (1987). *Biochemistry*, **26**, 8066–8072.
Teo, B. K. (1986). *EXAFS: Basic Principles and Data Analysis*. Berlin: Springer Verlag.
Tsukihara, T., Aoyama, H., Yamashita, E., Tomizaki, T., Yamaguchi, H., Shinzawa-Itoh, K., Nakashima, R., Yaono, R. & Yoshikawa, S. (1996). *Science*, **272**, 1136–1144.
Wang, H., Peng, G., Miller, L. M., Scheuring, E. M., George, S. J., Chance, M. R. & Cramer, S. P. (1997). *J. Am. Chem. Soc.* **119**, 4921–4928.
Wang, H., Ralston, C. Y., Patil, D. S., Jones, R. M., Gu, W., Verhagen, M., Adams, M., Ge, P., Riordan, C., Marganian, C. A., Mascharak, P., Kovacs, J., Miller, C. G., Collins, T. J., Brooker, S., Croucher, P. D., Wang, K., Steifel, E. I. & Cramer, S. P. (2000). *J. Am. Chem. Soc.* **122**, 10544–10552.
Wieghardt, K. (1989). *Angew. Chem. Int. Ed. Engl.* **28**, 1153–1172.
Yachandra, V. K. (1995). *Biochemical Spectroscopy*, *Methods in Enzymology*, Vol. 246, edited by K. Sauer, pp. 638–678. New York: Academic Press.
Yachandra, V. K., DeRose, V. J., Latimer, M. J., Mukerji, I., Sauer, K. & Klein, M. P. (1993). *Science*, **260**, 675–679.
Yachandra, V. K., Guiles, R. D., McDermott, A. E., Britt, R. D., Dexheimer, S. L., Sauer, K. & Klein, M. P. (1986). *Biochim. Biophys. Acta*, **850**, 324–332.
Zhabinsky, S. I., Rehr, J. J., Ankudinov, A., Albers, R. C. & Eller, M. J. (1995). *Phys. Rev. B*, **52**, 2995–3009.
Zouni, A., Witt, H.-T., Kern, J., Fromme, P., Krauß, N., Saenger, W. & Orth, P. (2001). *Nature* (*London*), **409**, 739–743.

Received 8 November 2001 • Accepted 29 August 2002